Redox-mediated zinc electrode for ultra-robust deep-cycle redox flow battery

Shiqiang Huang[a], Zhizhang Yuan[c], Manohar Salla[a], Xun Wang[a], Hang Zhang[a], Songpeng Huang[a], Dao Gen Lek[a], Xianfeng Li[c]* and Qing Wang[a, b,]*

[a] Department of Materials Science and Engineering, College of Design and Engineering, National University of Singapore, 117574, Singapore

[b] Institute of Materials Research and Engineering (IMRE), Agency for Science Technology and Research (A*STAR), Singapore, 138632, Singapore

[c] Division of Energy Storage, Dalian National Laboratory for Clean Energy, Dalian Institute of Chemical Physics, Chinese Academy of Sciences, Zhongshan Road 457, Dalian 116023, China

*e-mail: msewq@nus.edu.sg; lixianfeng@dicp.ac.cn

Materials and experimental details

Materials. All chemicals were purchased from Sigma-Aldrich and used without further purification. DHPS was synthesized using the method reported in literature.[1] Nafion 115 and Nafion 212 (Dupont) membrane were purchased from Chemours. The carbon felt was purchased from Liaoyang Jingu Carbide Co., Ltd or SGL Carbon and used as received.

Electrochemical measurements. Cyclic voltammetric (CV) measurements were carried out with an Autolab electrochemical workstation (Metrohm, PGSTAT30) using a three-electrode configuration composed of a glassy carbon working electrode, a platinum plate counter electrode and an Hg/HgO reference electrode. The glassy carbon working electrode was polished with 0.3 and 0.05 μm of alumina slurry for 2 minutes and then sonicated in deionized water before every test. To determine the overpotentials of different cell components, 4-electrode electrochemical characterization was performed, for which 60 mL of 0.6 M $Fe(CN)_6^{3-}$ /0.05 M $Fe(CN)_6^{4-}$/1.8 M OH^- and 20 mL 3.8 M OH^- with/without 7 mM DHPS + 0.1 g zinc plate was attached on the carbon felt used as the anode or 30 mL 3.8 M OH- with 20 mM DHPS were used as catholyte and the anolyte, respectively. Two Hg/HgO REs were inserted in both the positive and negative electrode compartments (see the setup shown in Figure 3c), the active area was 5 cm^2 and the current density was 30 mA/cm^2.

Zinc-based flow cell assembly and test. In zinc-based symmetric flow cell, zinc plate attached on carbon felt were used as both cathode and anode. In alkaline zinc-iron flow cell, carbon felt was served as cathode; A piece of zinc plate attached on carbon felt was employed as anode. Nafion 115 membrane was used to separate the catholyte and anolyte except for the rate tests which used Nafion 212 membrane. Viton gasket and PTFE tubing (Cole-Parmer) were employed to build the cell. The active area of carbon felt was 13.5 cm^2. The membranes were soaked in 3.8 M NaOH overnight prior to use. For the first discharge process, the current density should precisely be determined by the specific area of zinc metal, while for the subsequent cycles the apparent current density should be calculated by the specific area of carbon felt as the zinc deposited on the carbon felt. To avoid confusion, we have used the specific area of carbon felt (13.5 cm^2) to calculate the current density and areal capacity in this work. Zinc metal was used as the only zinc source at the anodic side for the discharge process. So, the capacity of anode is totally from the zinc metal and the DOD can be calculated based on the discharged capacity and theoretical capacity of zinc metal. For zinc-based symmetric flow cell with low areal capacity (12.2 mAh/cm^2), 20 mL and 60 mL 3.8 M NaOH with/without 20 mM DHPS and 0.3 M ZnO/3.8 M NaOH were used as anolyte and catholyte, respectively. 1.65 g of zinc was used for cathode and 0.2 g for anode, and the current density was 20 mA/cm^2. For zinc-based symmetric flow cell with high areal capacity (92 mAh/cm^2), 60 mL and 120 mL 3.8 M

NaOH with 20 mM DHPS and 0.3 M ZnO/3.8 M NaOH were used as anolyte and catholyte, respectively. 4.15 g of zinc was used for cathode and 1.5 g for anode, and the current density was 50 mA/cm^2. For zinc-iron flow battery with areal capacity of 152 mAh/cm^2, 110 mL and 300 mL 3.8 M OH^- with 30 mM DHPS and 0.6 M $Fe(CN)_6^{3-}$/0.05 M $Fe(CN)_6^{4-}$/1.8 M OH^- were used as anolyte and catholyte, respectively. 2.5 g of zinc was used for anode, and the current density was 50 mA/cm^2. For zinc-iron flow battery with areal capacity of 250 mAh/cm^2, 150 mL and 400 mL 3.8 M OH^- with 30 mM DHPS and 0.6 M $Fe(CN)_6^{3-}$/0.05 M $Fe(CN)_6^{4-}$/1.8 M OH^- were used as anolyte and catholyte, respectively. 4.10 g of zinc was used for anode, and the current density was 80 mA/cm^2. For the galvanostatic measurements, the batteries were charged to the theoretical capacity of zinc or a cutoff voltage, whichever is reached first, and discharged to a cutoff voltage. The galvanostatic measurements were performed with an Arbin battery tester.

Characterizations.

In situ UV-Vis spectra of the DHPS-mediated zinc oxidation reactions were collected with a SHIMADZU UV-1800 spectrometer (see the setup shown in Figure S6). A custom-designed spectroelectrochemical cell with 0.6 mm optical path length was connected to the outlet of the reaction tank. The absorbance changes of DHPS were recorded during the reaction process. For the chemical reaction test, the supporting electrolyte was 3.8 M NaOH and for the kinetics test, the supporting electrolyte was 0.4 M $Zn(OH)_4^{2-}$/3 M NaOH.

Operando FTIR measurement was carried out with a PerkinElmer Frontier MIR/FIR system by the Attenuated Total Reflection (ATR) model to detect the structural evolution of DHPS during different stages (see the setup shown in Figure S8). DHPS flowed through the ATR crystal and the FTIR spectra were collected from 1600 to 1000 cm^{-1} with a resolution of 4 cm^{-1}.

XRD measurements were conducted on a Powder XRD Diffractometer System (Bruker D8 Advance) and SEM measurements were conducted on Zeiss Supra 40.

"Dead zinc" calculation.

The quantity/capacity of the "dead zinc" is calculated by the areal capacity difference of DHPS between the discharge (second discharge plateau which includes the capacity of DHPS and "dead zinc") and the corresponding charge process (first charge plateau which only includes the capacity of DHPS):

$$C_{dead\ zinc} = C_{DHPS-discharge} - C_{DHPS-charge}$$

Table S1. Summary of some reported zinc-based redox flow batteries.

	Duration (h)	Areal capacity (mAh/cm^2)	Current density (mA/cm^2)	$Zn/Zn(OH)_4^{2-}/Zn^{2+}$ utilization (%)
Zn/Br				
Ref. [2]	100*	20	40	4.67%
Ref. [3]	50*	20	80	4.67%
Ref. [4]	700*	20	20	4.07%
Ref. [5]	383*	85	20	67.42%
Ref. [6]	100*	10	20	0.52%
Ref. [7]	284*	40	40	6.72%
Ref. [8]	50*	40	160	33.64%
Ref. [9]	2060*	20	100	4.48%
Ref. [10]	560*	40	80	5.60%
Zn/I				
Ref. [11]	1872**	234	10	66.60%
Ref. [12]	>2100	54	80	19.33%
Zn/Ce				
Ref. [13]	1203*	240	20	81%
Ref. [14]	75	3.125	25	0.35%
Zn/Fe (neutral)				
Ref. [15]	213**	42.5	40	79%
Zn/Fe (alkaline)				
Ref. [16]	375**	100	80	35%
Ref. [17]	583	53	80/160	66.4%
Ref. [18]	250	20	80	16.8%
Ref. [19]	1200	65	80	68%
	500	240	40	56%
Ref. [20]	800	66.7	80	70%
Ref. [21]	>400	160	80	N.A.
Ref. [22]	97.5	20	80/160	75%
Ref. [23]	>650	40/80	80/160	75%
This work	>1500	152 (up to 250)	50 (80 for 250 mAh/cm^2)	97.5%

*Estimated based on the charging capacity with CE=100% and no capacity decay
**Estimated based on the discharge capacity with CE=100% and no capacity decay

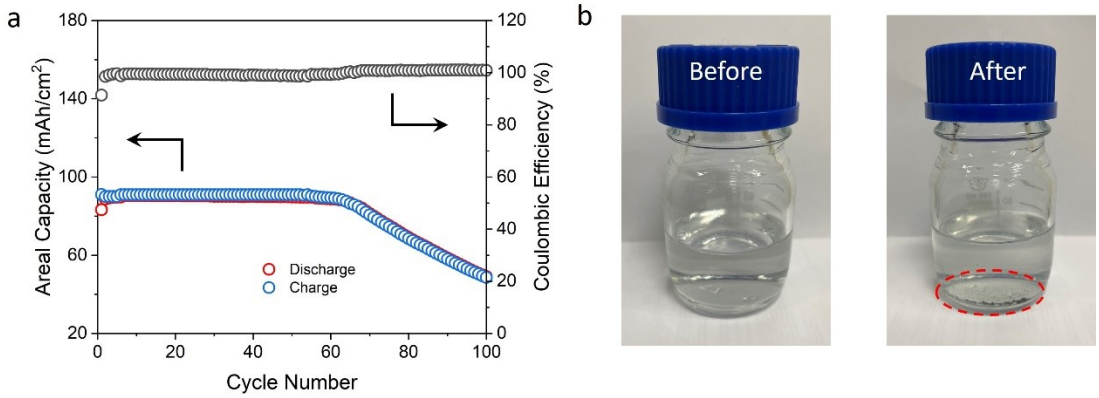

Figure S1. a, Cycling performance of a zinc-based symmetric flow cell with an areal capacity of 92 mAh/cm^2 at 50 mA/cm^2. b, Corresponding photographs of the anolyte at anodic tank before and after cycling at 50 mA/cm^2. Some silver-grey particles are observed after 101st cycling at the discharge state.

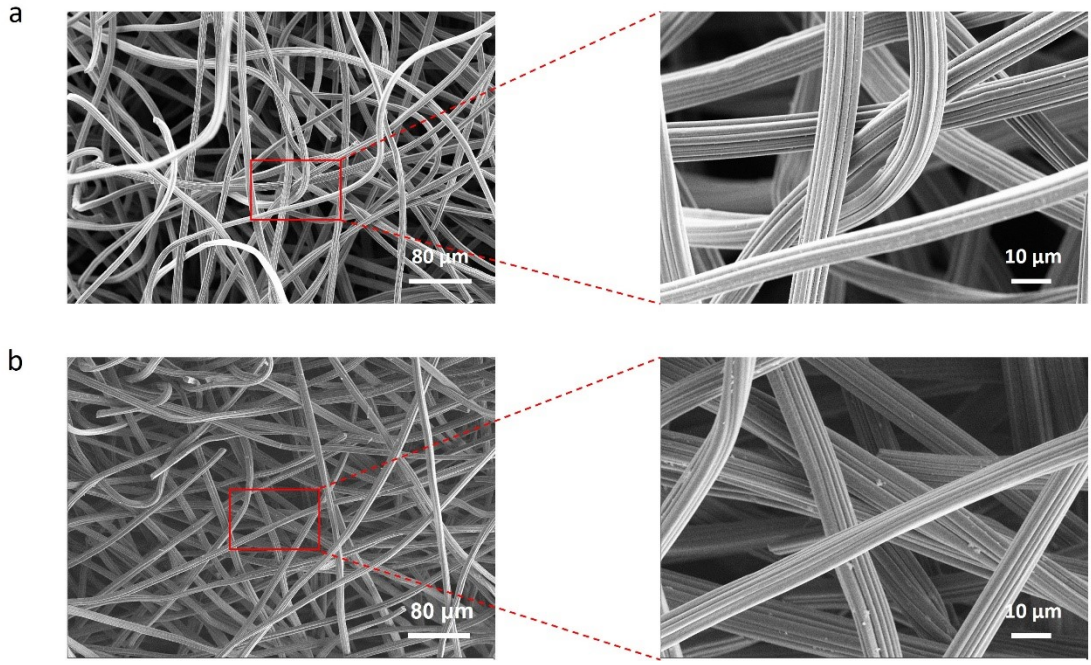

Figure S2. The SEM images of (a) the pristine carbon felt electrode and (b) the electrode after 101st cycling at the discharge state with current density of 50 mA/cm^2.

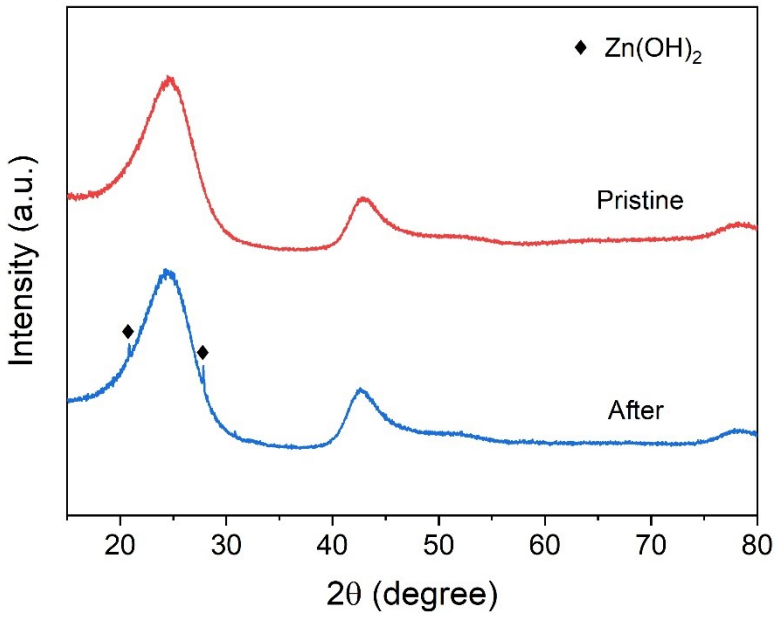

Figure S3. XRD patterns of pristine carbon felt electrode and the electrode after symmetric flow cells testing (stopped at discharge state after 101st cycle) at 50 mA/cm^2. The areal capacity of zinc in the cells is 92 mAh/cm^2.

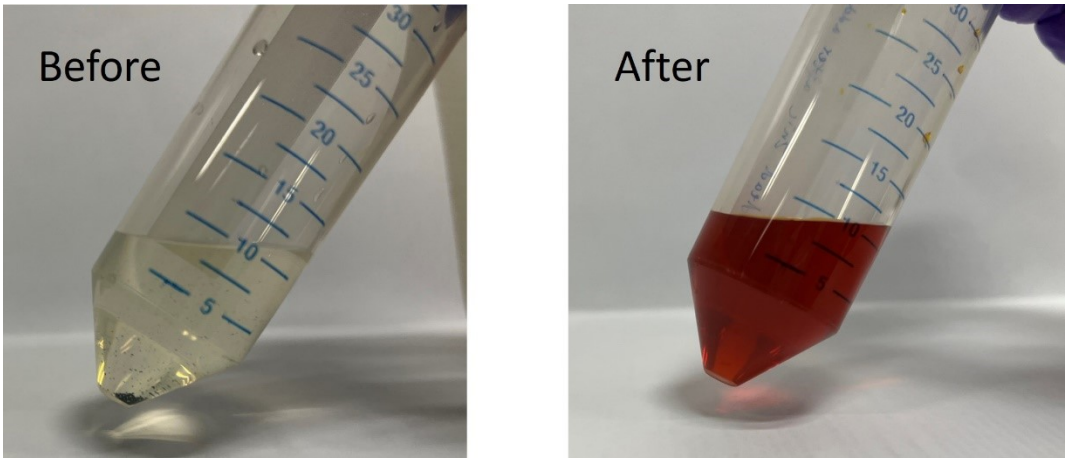

Figure S4. Photographs of anolytes with silver-grey particles before and after adding 20 mM DHPS.

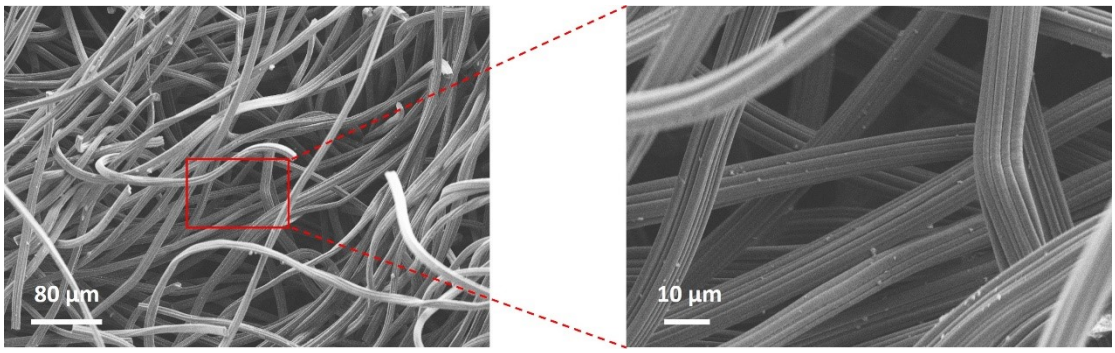

Figure S5. SEM images of the electrode after cycling, followed by immersion in anolyte with 20 mM DHPS for 24 h.

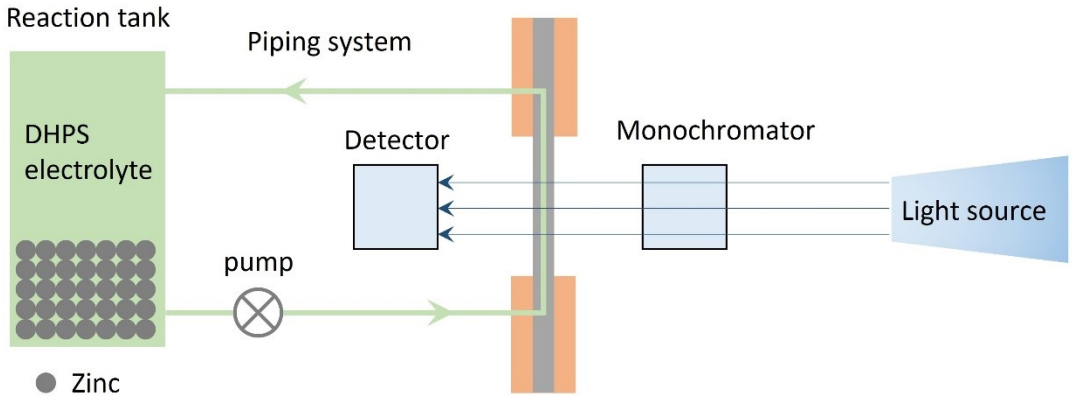

Figure S6. Configuration of the setup for in-situ UV-Vis measurement.

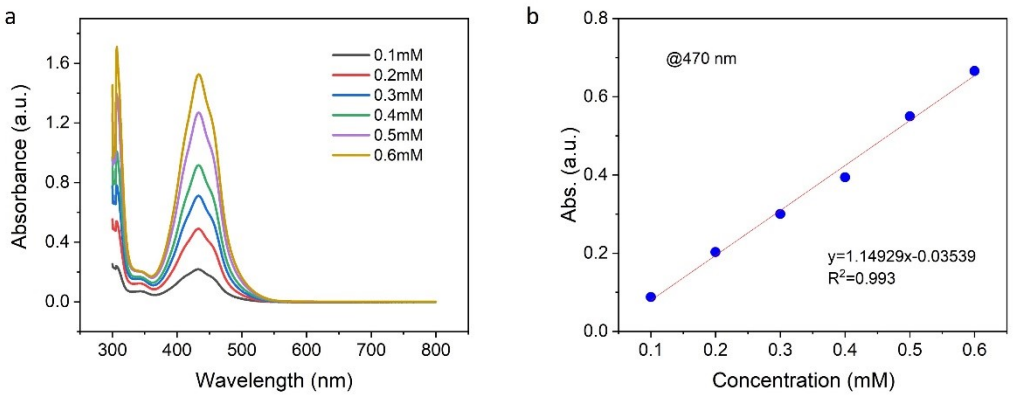

Figure S7. a, UV-vis spectra of DHPS in 3.8 M NaOH. The UV-vis spectra were recorded by using 3.8 M NaOH aqueous solution as the blank, and the optical path length is 1 mm. b, The corresponding standard curve obtained at the wavelength of 470 nm.

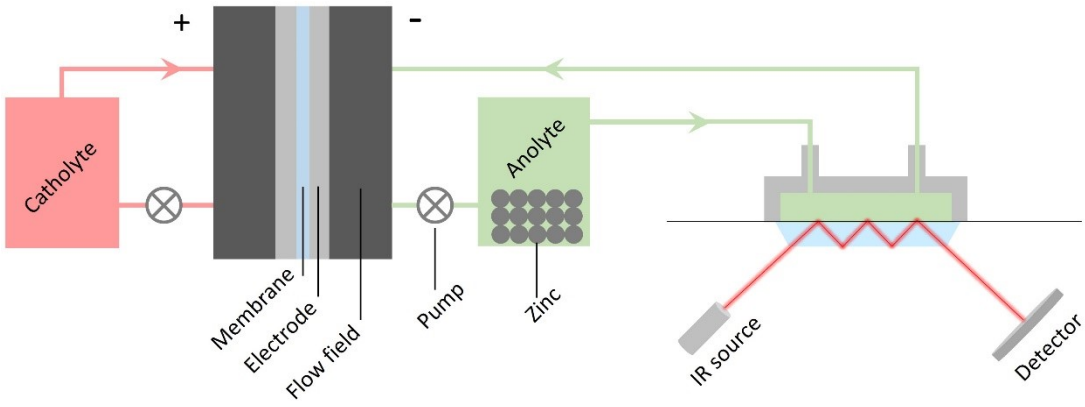

Figure S8. Configuration of the setup for operando ATR-FTIR measurement.

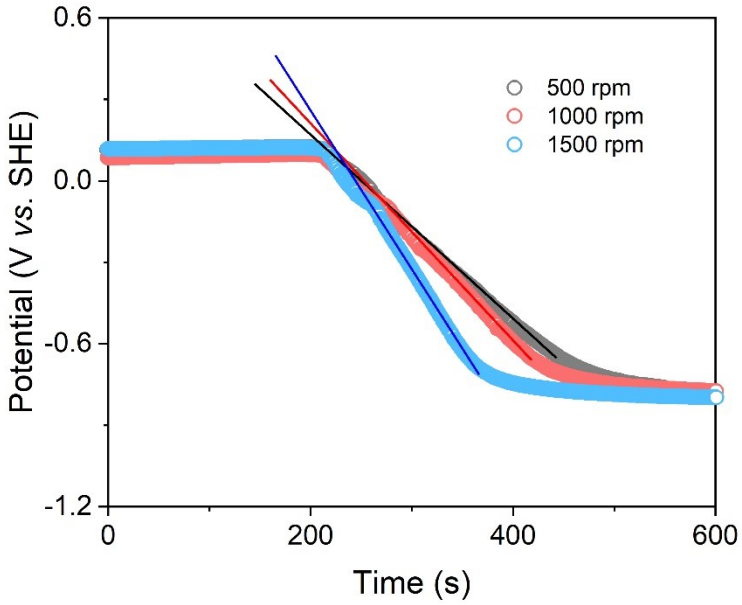

Figure S9. OCP changes of 60 mL DHPS-based solution (1 mM DHPS in 0.4 M ZnO/3.8 M NaOH) before and after adding excess zinc powder with the rotating speed of 500/1000/1500 rpm. The slopes were calculated to be -0.0032, -0.0036 and -0.0055 for 500/1000/1500 rpm, respectively.

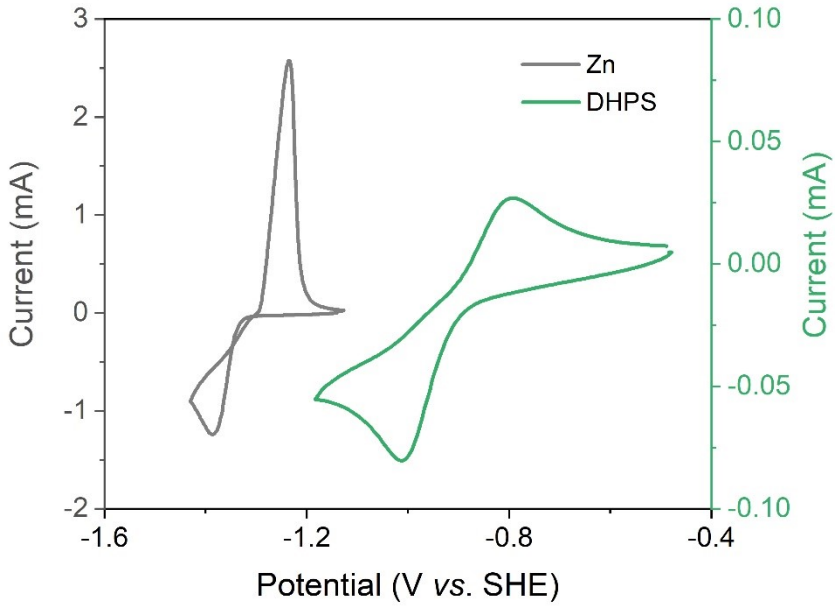

Figure S10. CV curves of 50 mM $[Zn(OH)_4]^{2-}$/3.8 M NaOH and 5 mM DHPS/3.8 M NaOH. Working electrode: glassy carbon disk; scan rate: 0.05 V/s.

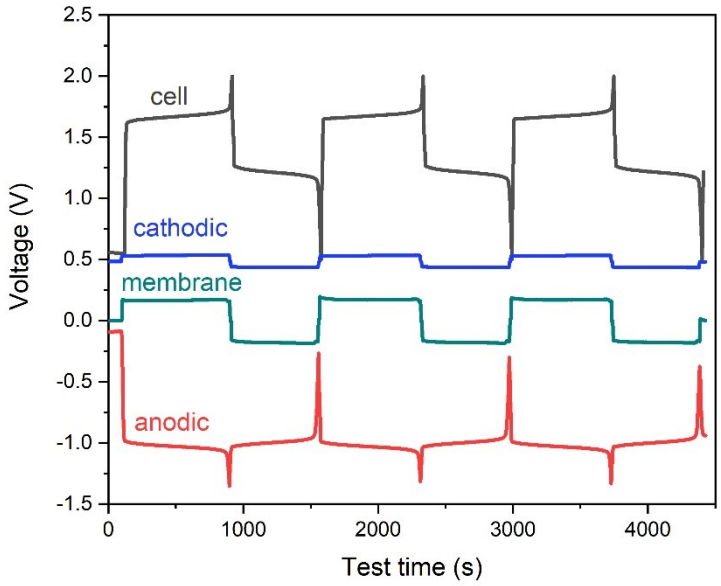

Figure S11. Four-electrode measurement of the various potential differences of a DHPS/$[Fe(CN)_6]^{3-/4-}$ flow cell at a current density of 30 mA/cm^2. As shown in the figure, the ΔV_+ and ΔV_- between charge and discharge processes are almost negligible and the main resistance is from membrane and other series resistance of the device.

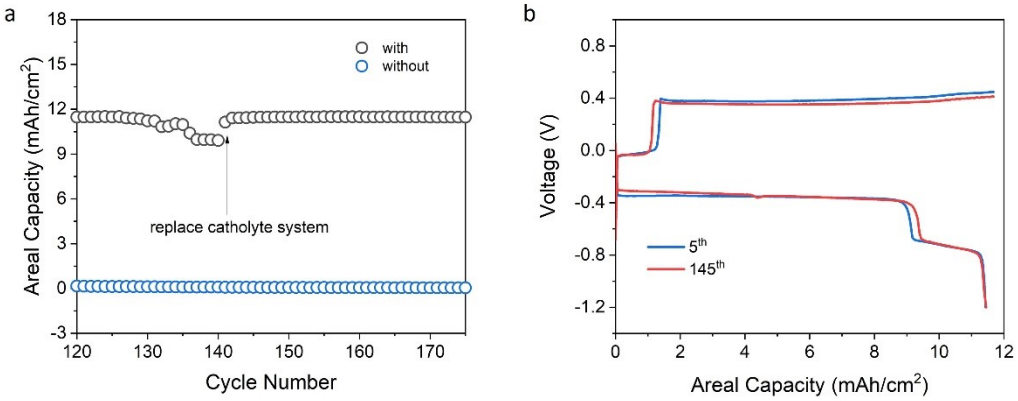

Figure S12. a, Cycling performance from 120 to 175 cycles of two zinc-based symmetric cells with a zinc areal capacity of 12.2 mAh/cm^2 with/without DHPS in anolyte. The catholyte system was replaced at the 140th cycle. b, The voltage curves of the cell at the 5th and 145th cycles. The current density was 20 mA/cm^2.

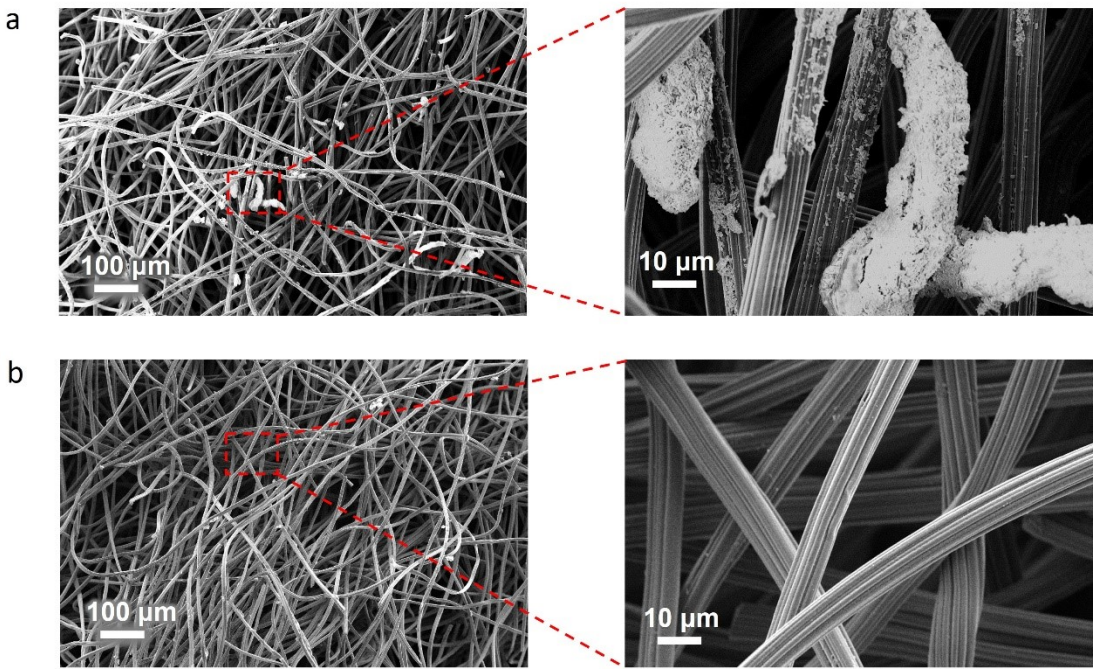

Figure S13. SEM images of the electrode (a) without and (b) with DHPS after 175 cycles (at discharge state) at 12.2 mAh/cm^2 under 20 mA/cm^2.

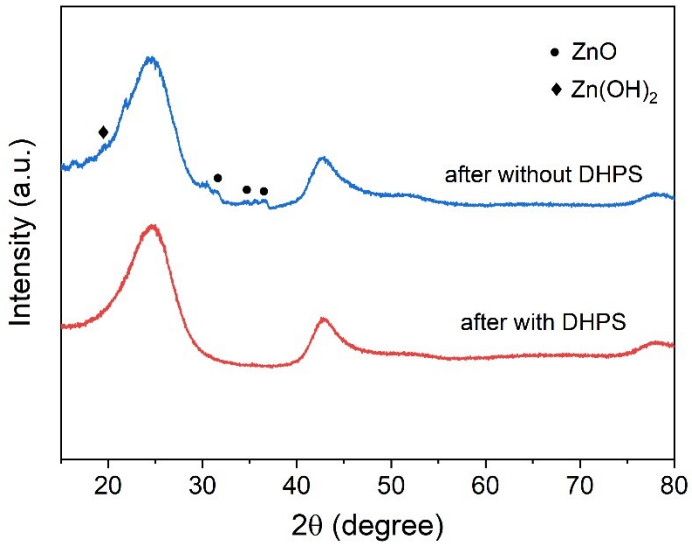

Figure S14. XRD patterns of carbon felt electrodes after testing for 175 cycles (at discharge state) at 20 mA/cm^2 without and with DHPS in anolyte. The areal capacity of zinc in the cells is 12.2 mAh/cm^2.

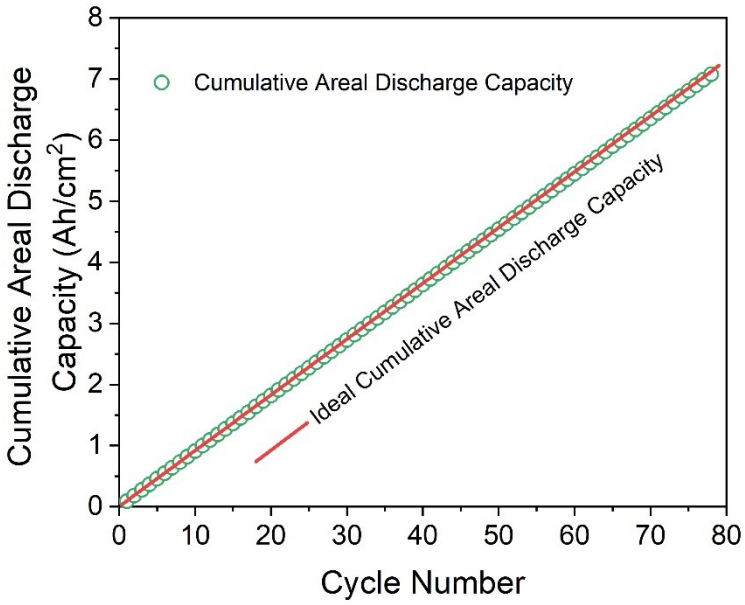

Figure S15. Cumulative discharge capacity of a DHPS-mediated zinc symmetric flow battery undergone 78 cycles (3rd to 80th cycle) of continuous testing (around 11.89 days) at a current density of 50 mA/cm^2. The theoretical capacity was calculated based on the 3rd areal discharge capacity (0.0912 Ah/cm^2) as the first two cycles may have some side reactions as observed in Figure 4c.

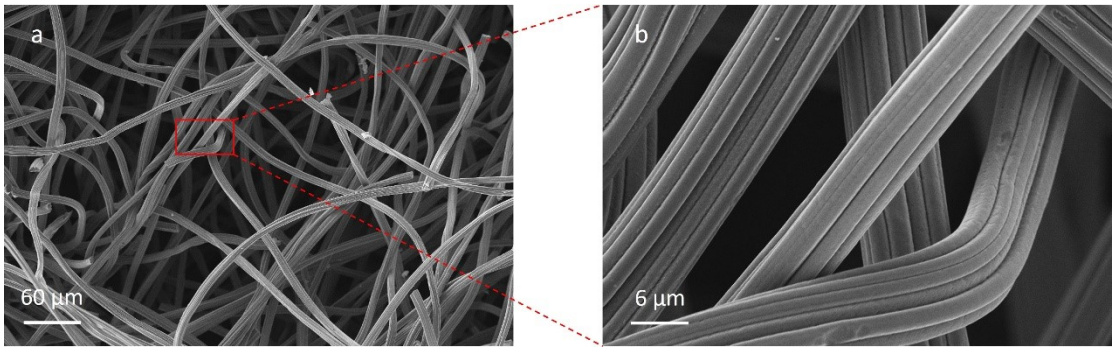

Figure S16. SEM images of carbon felt electrode with DHPS in anolyte after 80 cycles (at discharge state) at 92 mAh/cm^2 under 50 mA/cm^2.

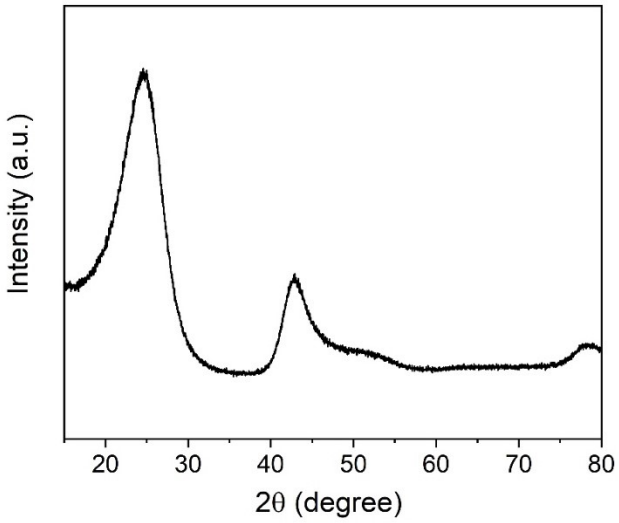

Figure S17. XRD pattern of carbon felt electrode with DHPS in anolyte after 80 cycles (at discharge state) at 92 mAh/cm^2 under 50 mA/cm^2.

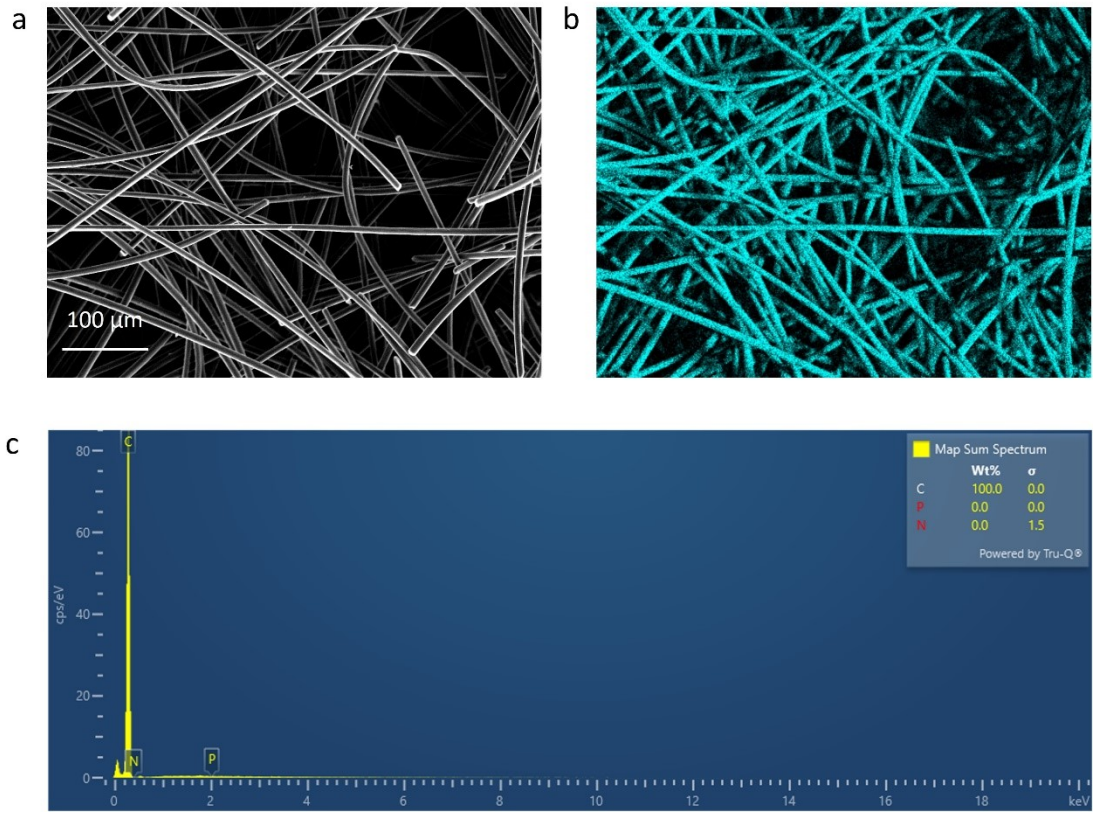

Figure S18. a, SEM image of carbon felt electrode from a redox-mediated AZIFB after 248 cycles (at discharge state) at 152 mAh/cm^2 under 50 mA/cm^2. b, EDS mapping for C element. c, EDX spectrum of carbon felt.

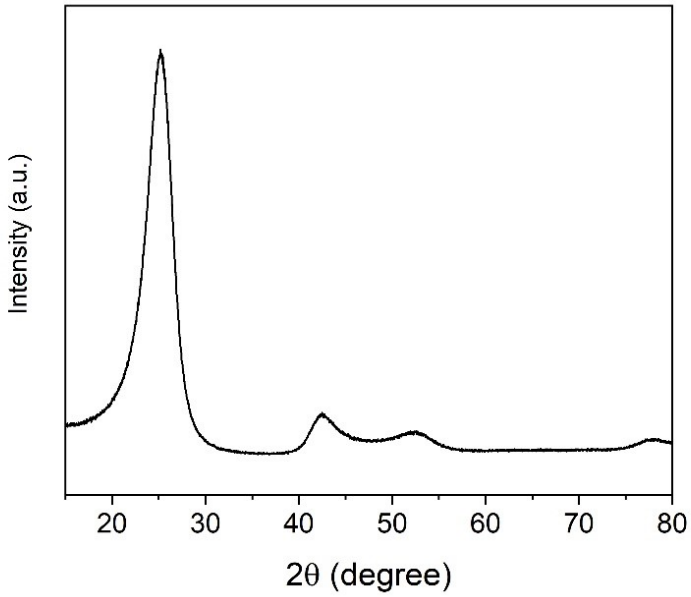

Figure S19. XRD pattern of carbon felt electrode from a redox-mediated AZIFB after 248 cycles (at discharge state) at 152 mAh/cm^2 under 50 mA/cm^2.

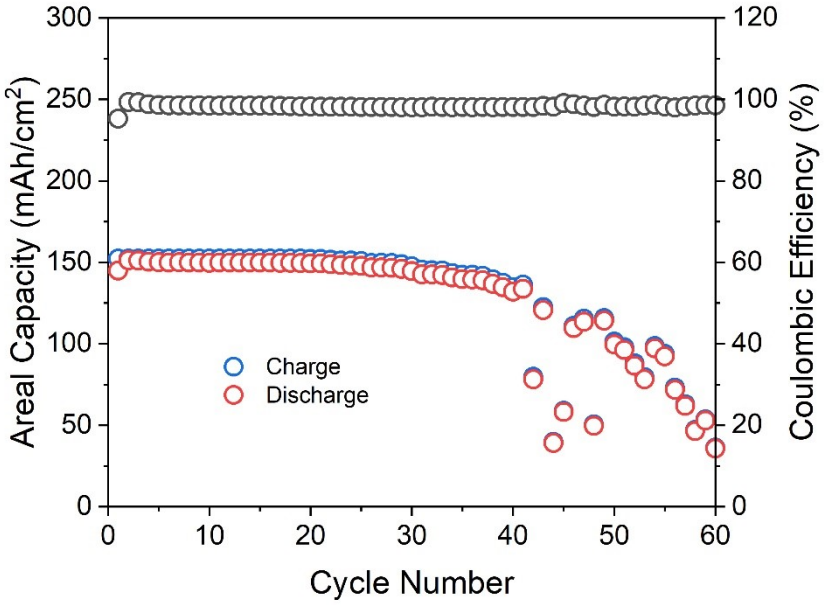

Figure S20. Cycling performance of a AZIFB with 152 mAh/cm^2 of zinc loading in the absence of DHPS in anolyte. The current density was 50 mA/cm^2.

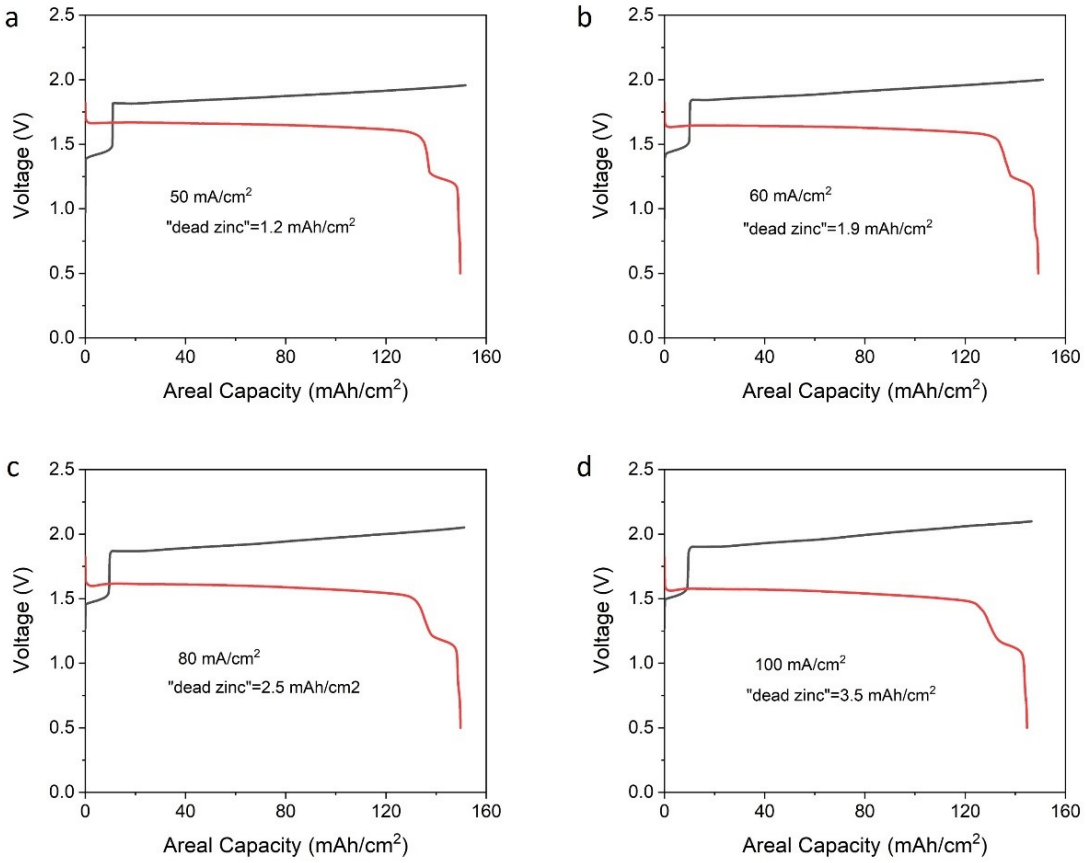

Figure S21. Voltage profiles of an AZIFB cycled at different current densities. The membrane was Nafion 212.

Table S2. Comparison of redox-mediated AZIFB and other advanced AZIFBs

	Redox-mediated AZIFB	Advanced AZIFBs[19]	
Depth of discharge/charge	Close to 100%	72%	56%
Voltage efficiency	87%	90%	95%
Cycling life (hour)	1500	1200	500
Coulombic efficiency	97.5%	98.0%	93.5%
Areal capacity (mAh/cm^2)	152	69	240
Current density (mA/cm^2)	50	80	40

Table S3. Comparison of redox-mediated AZIFB and other advanced aqueous redox-flow batteries

	Cell voltage (V)	Demonstrated cycling life (hour)	Demonstrated capacity fading rate		References
			%/day	%/cycle	
Acidic systems					
VRB	1.26	703*	1.09	0.024	24
Fe/Cr	1.18	46*	0.5	0.16	25
AQDS/Br	0.88	100	0.2	0.08	26
Neutral systems					
S_x^{2-}/I_x^-	1.05	>2088	0.005	0.0004	27
Zn/Mn	1.58	60	0	0	28
AQ-1,8-3E-OH/$Fe(CN)_6^{3-/4-}$	0.90	432	0.5	0.041	29
BTMAP-Vi/BTMAP-Fc	0.75	398	0.033	0.0011	30
Pyr-TEMPO/$[PyrPV]Cl_4$	1.57	360	3.47	0.05	31
Alkaline systems					
DPivOHAQ/$Fe(CN)_6^{3-/4-}$	0.98	384	0.0018	0.00004	32
ACA/$Fe(CN)_6^{3-/4-}$	1.13	129*	1.2	0.02	33
PFP/ $Fe(CN)_6^{3-/4-}$	1.15	1272	0	0	34
Redox-mediated Zn/$Fe(CN)_6^{3-/4-}$	1.73	>1500	0.019	0.0048	This work

*The demonstrated cycling life is estimated using the theoretical/first charge capacity without considering capacity decay: demonstrated cycling life = (theoretical/first charge capacity)/current*2*cycle number.

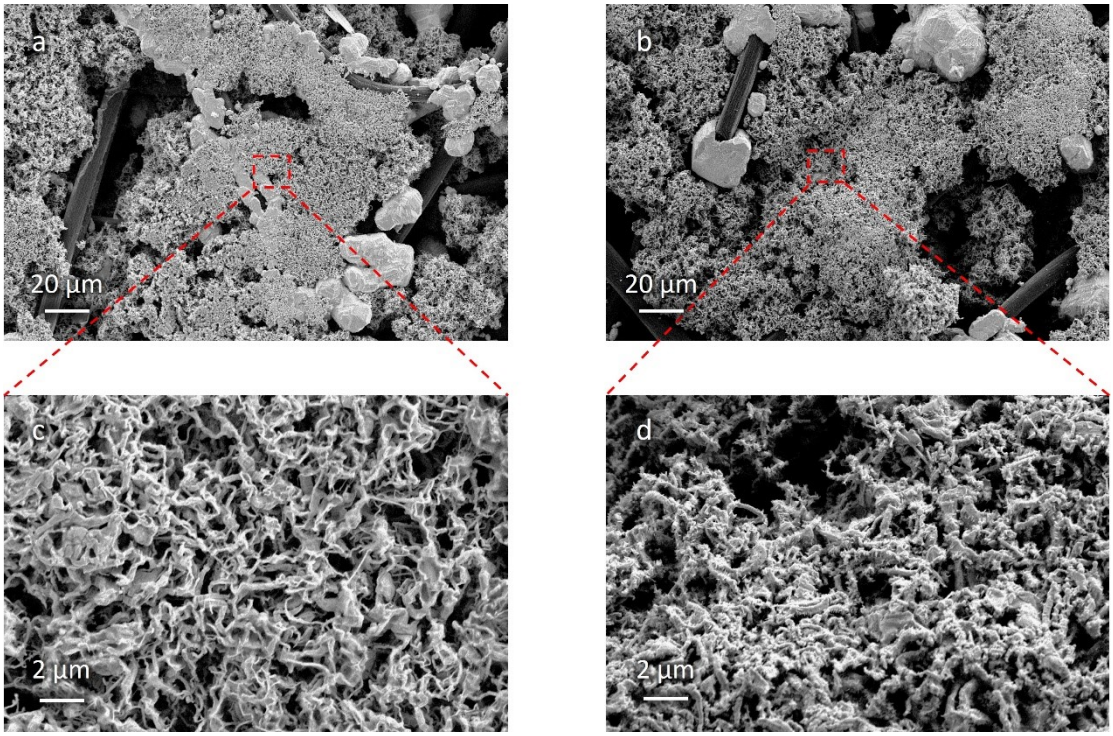

Figure S22. SEM images of the carbon felt electrode surface after charging to an areal capacity of 152 mAh/cm^2 at 50 mA/cm^2. (a,c) without DHPS and (b,d) with DHPS in anolyte.

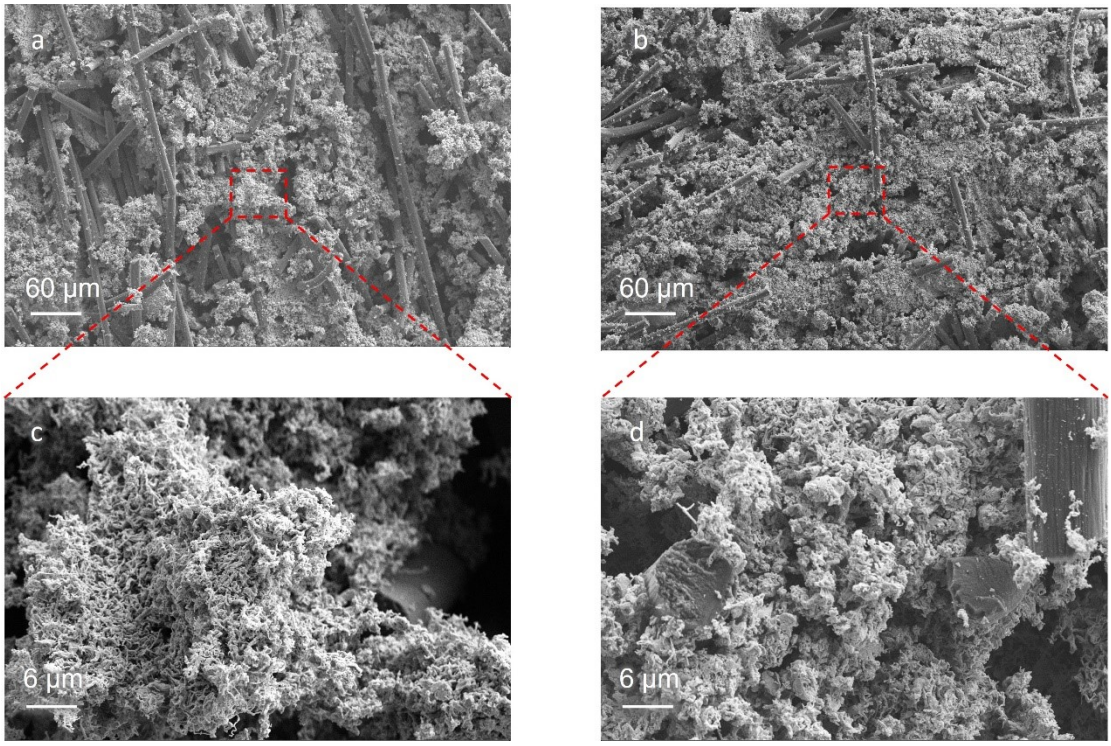

Figure S23. SEM images of the cross section of the carbon felt electrode after charging to an areal capacity of 152 mAh/cm^2 at 50 mA/cm^2. (a,c) without DHPS and (b,d) with DHPS in anolyte.

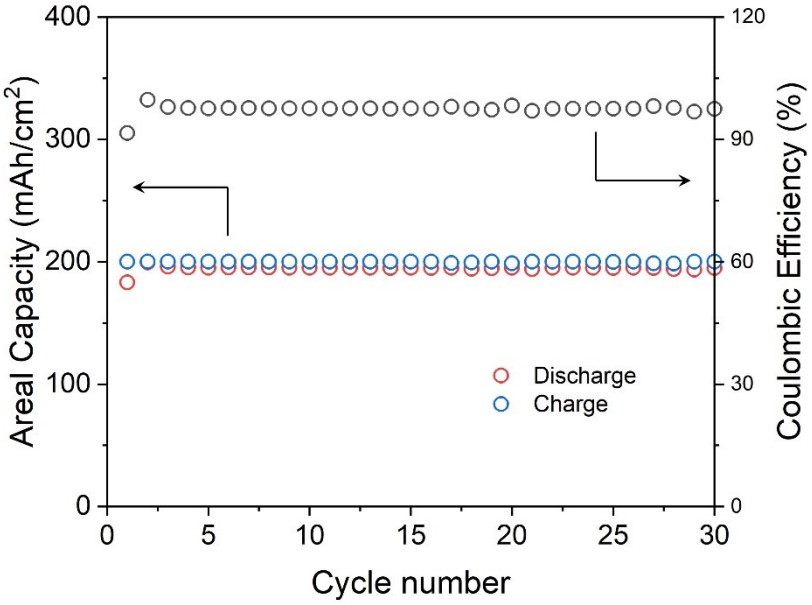

Figure S24. Cycling performance of an AZIFB with an areal zinc capacity of 200 mAh/cm^2 and 30 mM DHPS in anolyte at 80 mA/cm^2.

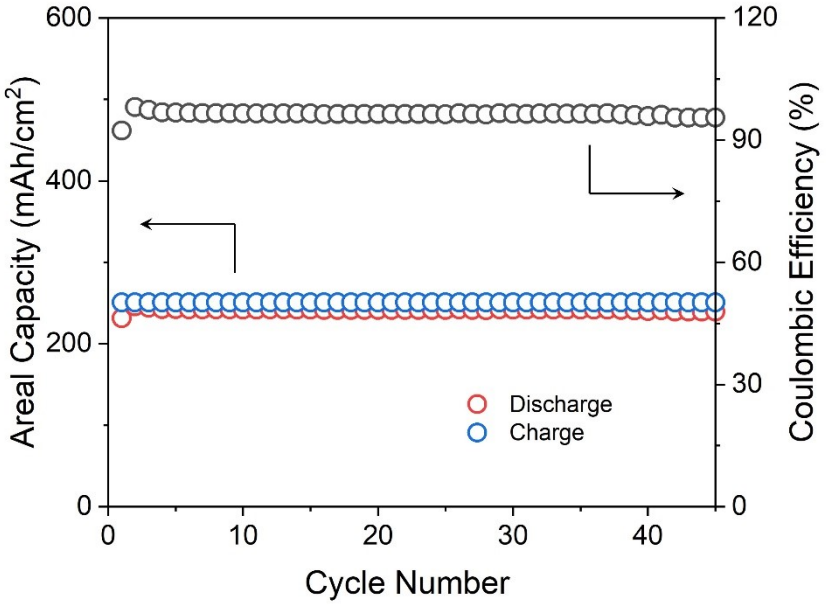

Figure S25. Cycling performance of an AZIFB with an areal zinc capacity of 250 mAh/cm^2 and 30 mM DHPS in anolyte at 80 mA/cm^2.

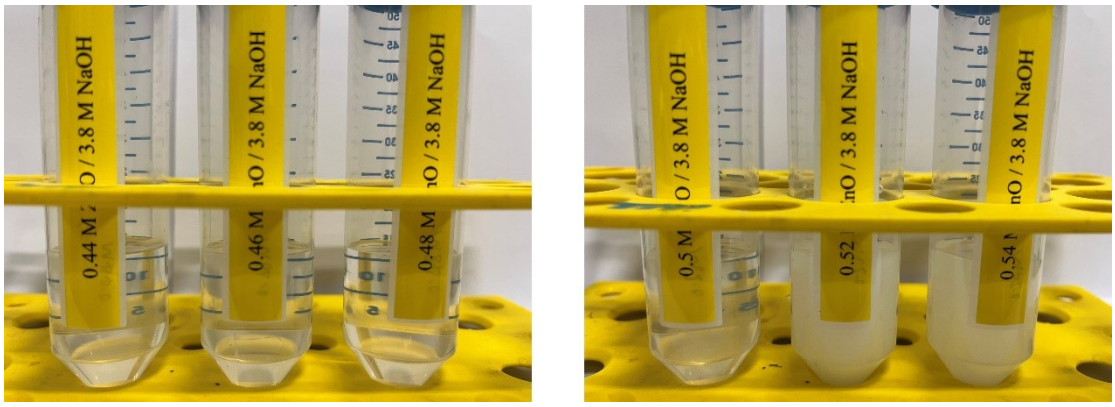

Figure S26. Solubility test of ZnO in 3.8 M NaOH. It was tested by dissolving ZnO into 15 mL 3.8 M NaOH solution until reaching saturated state. The solubility is around 0.5 M.

Supplementary Note: Analysis of AZIFB with high areal capacity.

Condition one: with the same power (P) requirement, where the active area (A) is 0.89 m^2, the current density (j) is 50 mA/cm^2 and voltage of single cell (U_0) is 1.5 V. Here we take 10 kW as an example:

$$P = U \times I = n \times U_0 \times j \times A = n \times 1.5 \times 0.05 \times 8900 = 10000$$

The number of single cells (n) is calculated to be 15.

The energy (E) can be calculated based on:

$$E = C \times U = n \times C_{Areal} \times A \times n \times U_0 = 15^2 \times 1.5 \times 8900 \times C_{Areal}$$

Here C_{Areal} is the areal capacity of a single cell.

For the battery with a low C_{Areal} of 20 mAh/cm^2, E was calculated to be around 60 kWh, which can continuously work for 6 h. For the battery with a high C_{Areal} of 200 mAh/cm^2, E was calculated to be around 600 kWh, which can continuously work for around 60 h.

As a result, the high areal capacity is beneficial for the long-duration operation when the power requirement is satisfied.

Condition two: with the same energy requirement while the basic power requirement is satisfied, where the active area (A) is 0.89 m^2, the current density (j) was 50 mA/cm^2 and voltage of single cell (U_0) is 1.5 V. Here we take 600 kWh as an example:

The energy (E) can be calculated based on:

$$E = C \times U = n \times C_{Areal} \times A \times n \times U_0 = n^2 \times 1.5 \times 8900 \times C_{Areal} = 600000$$

For the battery with a high C_{Areal} of 200 mAh/cm^2, the number of single cells (n) is calculated to be around 15. For the battery with a low C_{Areal} of 20 mAh/cm^2, n is calculated to be around 47.

As a result, to achieve the same energy density, the number of single cells increases from 15 to 47 when the areal capacity is reduced from 200 to 20 mAh/cm^2. Therefore, when the power requirement is satisfied, to achieve the same energy density, the larger areal capacity reduces the number of single cells in stack and accordingly lowers the cost considering the stack is one of the most expensive components for AZIFB.[35]

References:

1. Zhang F, Zhang H, Salla M, Qin N, Gao M, Ji Y*, et al.* Decoupled Redox Catalytic Hydrogen Production with a Robust Electrolyte-Borne Electron and Proton Carrier. *Journal of the American Chemical Society* 2021, **143**(1)**:** 223-231.
2. Wu MC, Zhao TS, Zhang RH, Wei L, Jiang HR. Carbonized tubular polypyrrole with a high activity for the Br2/Br− redox reaction in zinc-bromine flow batteries. *Electrochimica Acta* 2018, **284:** 569-576.
3. Wu MC, Jiang HR, Zhang RH, Wei L, Chan KY, Zhao TS. N-doped graphene nanoplatelets as a highly active catalyst for Br2/Br− redox reactions in zinc-bromine flow batteries. *Electrochimica Acta* 2019, **318:** 69-75.
4. Kim R, Yuk S, Lee J-H, Choi C, Kim S, Heo J*, et al.* Scaling the water cluster size of Nafion membranes for a high performance Zn/Br redox flow battery. *Journal of Membrane Science* 2018, **564:** 852-858.
5. Bae S, Lee J, Kim DS. The effect of Cr3+-Functionalized additive in zinc-bromine flow battery. *Journal of Power Sources* 2019, **413:** 167-173.
6. Suresh S, Ulaganathan M, Pitchai R. Realizing highly efficient energy retention of Zn–Br2 redox flow battery using rGO supported 3D carbon network as a superior electrode. *Journal of Power Sources* 2019, **438:** 226998.
7. Yin Y, Wang S, Zhang Q, Song Y, Chang N, Pan Y*, et al.* Dendrite-Free Zinc Deposition Induced by Tin-Modified Multifunctional 3D Host for Stable Zinc-Based Flow Battery. *Advanced Materials* 2020, **32**(6)**:** 1906803.
8. Wang C, Lu W, Lai Q, Xu P, Zhang H, Li X. A TiN Nanorod Array 3D Hierarchical Composite Electrode for Ultrahigh-Power-Density Bromine-Based Flow Batteries. *Advanced Materials* 2019, **31**(46)**:** 1904690.
9. Lee J-H, Kim R, Kim S, Heo J, Kwon H, Yang JH*, et al.* Dendrite-free Zn electrodeposition triggered by interatomic orbital hybridization of Zn and single vacancy carbon defects for aqueous Zn-based flow batteries. *Energy & Environmental Science* 2020, **13**(9)**:** 2839-2848.
10. Lu W, Xu P, Shao S, Li T, Zhang H, Li X. Multifunctional Carbon Felt Electrode with N-Rich Defects Enables a Long-Cycle Zinc-Bromine Flow Battery with Ultrahigh Power Density. *Advanced Functional Materials* 2021, **31**(30)**:** 2102913.
11. Li B, Nie Z, Vijayakumar M, Li G, Liu J, Sprenkle V*, et al.* Ambipolar zinc-polyiodide electrolyte for a high-energy density aqueous redox flow battery. *Nature Communications* 2015, **6**(1)**:** 6303.
12. Xie C, Zhang H, Xu W, Wang W, Li X. A Long Cycle Life, Self-Healing Zinc–Iodine Flow Battery with High Power Density. *Angewandte Chemie International Edition* 2018, **57**(35)**:** 11171-11176.
13. Xie Z, Liu B, Xie C, Yang B, Jiao Y, Cai D*, et al.* Chemically reduced graphene oxide paper as positive electrode for advanced Zn/Ce redox flow battery. *Materials Chemistry and Physics* 2018, **220:** 208-215.
14. Amini K, Pritzker MD. Improvement of zinc-cerium redox flow batteries using mixed methanesulfonate-chloride negative electrolyte. *Applied Energy* 2019, **255:** 113894.
15. Xie C, Duan Y, Xu W, Zhang H, Li X. A Low-Cost Neutral Zinc–Iron Flow Battery with High Energy Density for Stationary Energy Storage. *Angewandte Chemie International Edition* 2017, **56**(47)**:** 14953-14957.
16. Chen D, Kang C, Duan W, Yuan Z, Li X. A non-ionic membrane with high performance for alkaline zinc-iron flow battery. *Journal of Membrane Science* 2021, **618:** 118585.
17. Yuan Z, Duan Y, Liu T, Zhang H, Li X. Toward a Low-Cost Alkaline Zinc-Iron Flow Battery with a Polybenzimidazole Custom Membrane for Stationary Energy Storage. *iScience* 2018, **3:** 40-49.
18. Chang N, Yin Y, Yue M, Yuan Z, Zhang H, Lai Q*, et al.* A Cost-Effective Mixed Matrix Polyethylene Porous Membrane for Long-Cycle High Power Density Alkaline Zinc-Based Flow Batteries. *Advanced Functional Materials* 2019, **29**(29)**:** 1901674.

19. Hu J, Yuan C, Zhi L, Zhang H, Yuan Z, Li X. In Situ Defect-Free Vertically Aligned Layered Double Hydroxide Composite Membrane for High Areal Capacity and Long-Cycle Zinc-Based Flow Battery. *Advanced Functional Materials* 2021, **31**(31)**:** 2102167.
20. Hu J, Yue M, Zhang H, Yuan Z, Li X. A Boron Nitride Nanosheets Composite Membrane for a Long-Life Zinc-Based Flow Battery. *Angewandte Chemie International Edition* 2020, **59**(17)**:** 6715-6719.
21. Wu J, Yuan C, Li T, Yuan Z, Zhang H, Li X. Dendrite-Free Zinc-Based Battery with High Areal Capacity via the Region-Induced Deposition Effect of Turing Membrane. *Journal of the American Chemical Society* 2021, **143**(33)**:** 13135-13144.
22. Yuan Z, Liu X, Xu W, Duan Y, Zhang H, Li X. Negatively charged nanoporous membrane for a dendrite-free alkaline zinc-based flow battery with long cycle life. *Nature Communications* 2018, **9**(1)**:** 3731.
23. Yuan Z, Liang L, Dai Q, Li T, Song Q, Zhang H*, et al.* Low-cost hydrocarbon membrane enables commercial-scale flow batteries for long-duration energy storage. *Joule* 2022, **6**(4)**:** 884-905.
24. Yuan Z, Duan Y, Zhang H, Li X, Zhang H, Vankelecom I. Advanced porous membranes with ultra-high selectivity and stability for vanadium flow batteries. *Energy & Environmental Science* 2016, **9**(2)**:** 441-447.
25. Wang S, Xu Z, Wu X, Zhao H, Zhao J, Liu J*, et al.* Excellent stability and electrochemical performance of the electrolyte with indium ion for iron–chromium flow battery. *Electrochimica Acta* 2021, **368:** 137524.
26. Huskinson B, Marshak MP, Suh C, Er S, Gerhardt MR, Galvin CJ*, et al.* A metal-free organic–inorganic aqueous flow battery. *Nature* 2014, **505**(7482)**:** 195-198.
27. Li Z, Lu Y-C. Polysulfide-based redox flow batteries with long life and low levelized cost enabled by charge-reinforced ion-selective membranes. *Nature Energy* 2021, **6**(5)**:** 517-528.
28. Xie C, Li T, Deng C, Song Y, Zhang H, Li X. A highly reversible neutral zinc/manganese battery for stationary energy storage. *Energy & Environmental Science* 2020, **13**(1)**:** 135-143.
29. Jin S, Jing Y, Kwabi DG, Ji Y, Tong L, De Porcellinis D*, et al.* A Water-Miscible Quinone Flow Battery with High Volumetric Capacity and Energy Density. *ACS Energy Letters* 2019, **4**(6)**:** 1342-1348.
30. Beh ES, De Porcellinis D, Gracia RL, Xia KT, Gordon RG, Aziz MJ. A Neutral pH Aqueous Organic–Organometallic Redox Flow Battery with Extremely High Capacity Retention. *ACS Energy Letters* 2017, **2**(3)**:** 639-644.
31. Pan M, Gao L, Liang J, Zhang P, Lu S, Lu Y*, et al.* Reversible Redox Chemistry in Pyrrolidinium-Based TEMPO Radical and Extended Viologen for High-Voltage and Long-Life Aqueous Redox Flow Batteries. *Advanced Energy Materials* 2022, **12**(13)**:** 2103478.
32. Wu M, Jing Y, Wong AA, Fell EM, Jin S, Tang Z*, et al.* Extremely Stable Anthraquinone Negolytes Synthesized from Common Precursors. *Chem* 2020, **6**(6)**:** 1432-1442.
33. Lin K, Gómez-Bombarelli R, Beh ES, Tong L, Chen Q, Valle A*, et al.* A redox-flow battery with an alloxazine-based organic electrolyte. *Nature Energy* 2016, **1**(9)**:** 16102.
34. Xu J, Pang S, Wang X, Wang P, Ji Y. Ultrastable aqueous phenazine flow batteries with high capacity operated at elevated temperatures. *Joule* 2021, **5**(9)**:** 2437-2449.
35. Moore MA, Counce RM, Watson JS, Zawodzinski TA. A Comparison of the Capital Costs of a Vanadium Redox-Flow Battery and a Regenerative Hydrogen-Vanadium Fuel Cell. 2015; 2015.